



### Both Control and PMD iPSCs Induce Oligodendrocyte Lineage Cells In Vitro

Based on the previously reported methods for inducing OLs from human ESCs and iPSCs (Hu et al., 2009; Izrael et al., 2007; Kang et al., 2007), we established our own culture protocol to induce OLs by modifying previously established protocols for efficiently differentiating human ESCs and iPSCs into neural stem/progenitor cells (NS/PCs) as neurospheres through EB formation (Nori et al., 2011; Okada et al., 2008). First, dorsomorphin (a bone morphogenetic protein signal inhibitor), SB431542 (a transforming growth factor  $\beta$  [TGF- $\beta$ ] receptor inhibitor), and BIO (a GSK3 inhibitor) were added during the early phase of EB formation to facilitate differentiation into NS/PCs more efficiently. Quantitative RT-PCR analysis of the expression of the NS/PC marker *SOX1* in EBs revealed a significantly higher induction efficiency of NS/PCs in our protocol with DSB (DSB: dorsomorphin, SB431542, and BIO) compared with those in our previously established methods (control, DSB $-$ ) or those in the previously reported dual Smad inhibition with DS (Figure 2B). We also added retinoic acid for caudalization and purmorphamine (Sonic hedgehog agonist) for ventralization during EB formation until EB dissociation. Then, the dissociated EBs were cultured in suspension to form neurospheres in proliferation medium supplemented with factors that promote the commitment and proliferation of OL lineage cells (Shimada et al., 2012). For adherent differentiation, neurospheres were cultured in differentiation medium supplemented with factors that promote the commitment of OL lineage cells as indicated in the **Experimental Procedures** (Figure 2A). From the quantitative RT-PCR analysis in this protocol, the pluripotent marker (*NANOG*) was notably downregulated in the EB stage, and other lineage markers (mesodermal and endodermal markers, such as *BRACHYURY* and *SOX17*) were not detected in any stage.

The NS/PC marker (*SOX1*) was upregulated in the EB and neurosphere stages and gradually downregulated after adherent differentiation (differentiation stage; Figure 2C). The expression profiles were similar between the control, PMD1, and PMD2 iPSCs (Figure S1A available online). To reveal the differentiation potentials of neurospheres, we performed immunocytochemistry of differentiated neurospheres for markers of neurons ( $\beta$ III tubulin), astrocytes (GFAP), and oligodendrocytes (O4; Figures 2E and 2F) and a time course analysis of the expression levels of neuronal and glial markers through quantitative RT-PCR (Figure 2D). The expression profiles were similar between the control and PMD1 and PMD2 cells (Figure S1B). Based on these analyses, we confirmed the differentiation potentials of the iPSCs into three neural lineage cells and the reproducibility of our differentiation protocol. Regarding the differentiation potentials of OL lineage cells, all PMD-iPSCs and control iPSCs were able to induce platelet-derived growth factor receptor  $\alpha$  (PDGFR $\alpha$ )-OL progenitor cells (OPCs), O4 $^{+}$ -immature OLs (immature OLs), and myelin basic protein (MBP) $^{+}$ -mature OLs (mature OLs) with typical morphologies (Figure 3B). OPCs were also positive for NG2 (Figure 3A). In contrast, myelin protein zero (MPZ)-positive cells, a major structural protein of peripheral myelin, could not be detected, indicating that these cells were oligodendrocytes, but not schwann cells.

After 55–70 days in vitro (DIV), OPCs were observed in 86.3% of the colonies of control cells and 95.1% and 90.5% of the colonies of PMD1 and PMD2 cells, respectively. At 70–85 DIV, immature OLs were observed in 77.8% of control colonies and 93.8% and 93.8% of the colonies of PMD1 and PMD2 cells, respectively. At 80–95 DIV, mature OLs were observed in 74.9% of the colonies of control cells and 93.8% and 89.2% of the colonies of PMD1 and PMD2 cells, respectively (Figure 3C). No significant

### Figure 1. Features of the PMD Patients and Characterization of iPSCs

(A) MRI images of the brains of patient PMD1 (right) and an age-matched control (left). Mild and diffuse atrophy of the brain, dilatation of the ventricles (open arrow), and diffuse high-intensity signals in the white matter (open arrowhead) are shown. T1WI, T1-weighted images; T2WI, T2-weighted images.

(B) Direct sequencing analysis of genomic DNA from PMD1's leukocytes showed a missense mutation c.757 T > A (p.Ser253Thr) in exon 6 of the *PLP1* gene.

(C) Schematic representation of the mutation sites in PMD1 and PMD2.

(D) Representative morphology of iPSC colonies (above) and immunochemical analysis of pluripotent markers, *NANOG* and *OCT4* (below). The scale bars represent 200  $\mu$ m.

(E) Quantitative RT-PCR analysis of the expression of retroviral transgenes in established PMD iPSC clones. Data are presented as the mRNA copy numbers for each transgene divided by those for  $\beta$ -actin.

(F) Representative H&E staining of teratomas derived from established PMD iPSC clones. Teratomas were formed via the injection of undifferentiated iPSCs into the testes of NOD/SCID mice. Open arrow, neural rosettes. Arrowhead, pigmented epitheliums. Asterisks, goblet cells. Arrow, bones. Open arrowhead, cartilage. The scale bars represent 200  $\mu$ m.

(G) Representative pyrosequencing analysis of the mutations in the *PLP1* gene in fibroblasts and iPSCs. Identical mutations to those observed in the patients' fibroblasts (PMD1, 757 T > A; PMD2, 643 C > T) were confirmed in all the iPSC clones.

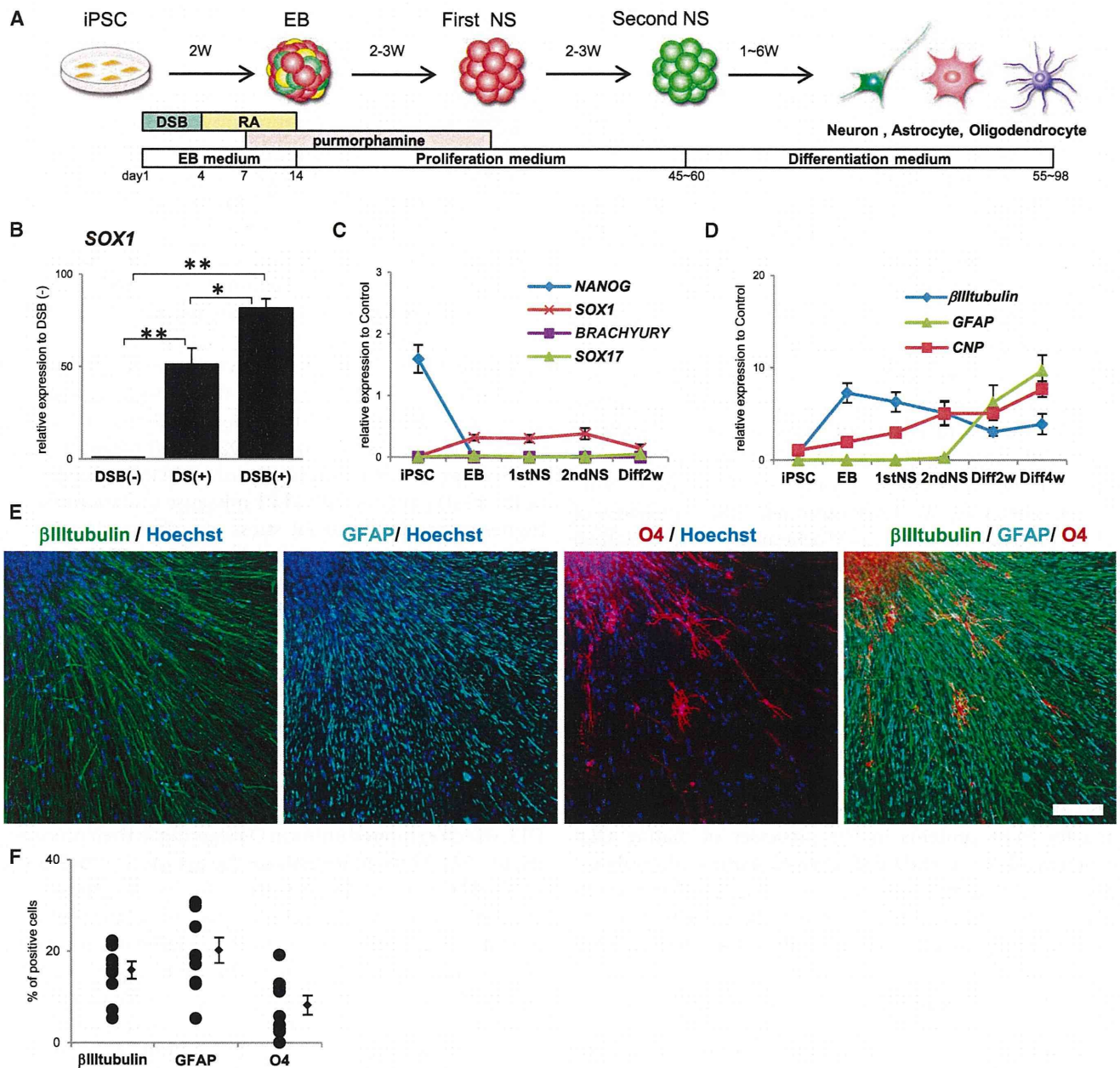


### Figure 2. Differentiation Potential of Human iPSCs

(A) Schematic presentation of the protocols for OL differentiation from hiPSCs. DSB, dorsomorphine (D), SB431542 (S), and BIO (B); RA, retinoic acid; NS, neurospheres.

(B) Quantitative RT-PCR analysis of *SOX1* expression in EBs, suggesting a significantly higher induction efficiency of NS/PCs in EBs in our protocol with DSB (DSB: dorsomorphin, SB431542, and BIO) compared with those in our previously established methods (control, DSB-) or those in the previously reported method with dual Smad inhibition (DS) ( $n = 3$ , mean  $\pm$  SEM; independent experiments; \* $p < 0.05$ ; \*\* $p < 0.01$ ; t test).

(C) Quantitative RT-PCR analysis of the expression of cell-type-specific markers at each differentiation stage. *NANOG* (a pluripotent marker) was readily downregulated in the EB stage. Other lineage markers (mesodermal and endodermal markers, such as *BRACHYURY* and *SOX17*) were not detected in any stage. *SOX1* was upregulated in EB and neurosphere stage in control iPSC clones (201B7, WD39, and TIG121;  $n = 3$ ; mean  $\pm$  SEM; independent experiments).

(D) Quantitative RT-PCR analysis of differentiated neurospheres for the markers of neurons ( *$\beta$ III tubulin*), astrocytes (*GFAP*), and oligodendrocytes (*CNP*) in control iPSC clones (201B7, WD39, and TIG121;  $n = 3$ ; mean  $\pm$  SEM; independent experiments).

(legend continued on next page)



differences were detected in either control or PMD with regard to OL lineage differentiation efficiency.

To examine the proportion of immature and mature OL lineage cells, we performed immunocytochemistry for OLIG2, PDGFR $\alpha$ , and MBP after 2 or 4 weeks differentiation of control-iPSC-derived second neurospheres containing more than 40 OLIG2-positive cells and counted the number of marker-positive cells (Figures 3D and 3E). After 2 and 4 weeks of differentiation, OLIG2<sup>+</sup> and PDGFR $\alpha$ <sup>+</sup> OPCs were abundantly observed. After 4 weeks of differentiation, small numbers of MBP<sup>+</sup> mature OLs appeared.

### Involvement of ER Stress in PMD

Previous *in vitro* transfection studies in nonglial cells have indicated that various PLP1 mutants accumulate in the ER immediately after translation, in contrast to the distribution of wild-type PLP1 at the plasma membrane (Gow et al., 1994; Gow and Lazzarini, 1996; Thomson et al., 1997). Therefore, we next examined the expression of PLP1 proteins via immunocytochemistry. When stained with anti-PLP1 and MBP antibodies, the membrane protein PLP1 was observed to be dispersed into the processes of OLs and to colocalize with MBP in control iPSC-derived mature OLs. However, in PMD1 and PMD2 iPSC-derived mature OLs, PLP1 protein staining was not observed in the OL processes; instead, PLP1 protein staining localized to the perinuclear cytoplasm (Figure 4A). Thus, we also performed staining for the ER marker KDEL and found that the mislocalized PLP1 proteins colocalized with KDEL (Figures 4A and 4B). All of the control iPSC-derived OLs showed staining for PLP1 proteins in the processes of mature OLs, whereas all of the PMD iPSC-derived mature OLs only exhibited PLP1 protein localization in the ER. These results suggest that mutant PLP1 proteins accumulated in the ER and triggered ER stress in mature OLs derived from PMD-iPSCs.

We next examined the expression of ER stress markers in OLs. O4<sup>+</sup> cells were isolated from both the PMD and control iPSC-derived differentiated cells 4 weeks after the attachment of the second neurospheres via magnetic-activated cell sorting (MACS) using an anti-O4 antibody. The purified O4<sup>+</sup> cells underwent quantitative RT-PCR to determine the expression of ER stress markers (*BIP*, *CHOP*, and spliced *XBP1*). No significant differences were detected between the control and PMD iPSC-derived OLs regarding the expression of ER stress markers under default conditions (Figure 4C). Therefore, we next examined the susceptibility

of the iPSC-derived OLs to the extrinsic ER stress induced by treatment with a low concentration of tunicamycin 50 nM for 6 hr (known as an ER-stress inducer). The results showed that the expression of all ER-stress markers was significantly increased in tunicamycin-treated O4<sup>+</sup> cells relative to untreated O4<sup>+</sup> cells in PMD1 (Figure 4D). This result suggested that a higher susceptibility to ER stress was observed in PMD1 iPSC-derived OLs than in those derived from control and PMD2 iPSCs.

We next treated the iPSC-derived OLs with a higher concentration of tunicamycin 100 nM for 6 hr and examined the expression levels of ER stress markers. PMD2 iPSC-derived OLs showed significantly higher expression levels of spliced *XBP1*, the most sensitive ER stress marker, than control iPSC-derived OLs (Figure 4E). No significant differences were detected in the expression levels of *BIP* and *CHOP* between control and PMD2. Taken together, these results suggest that ER stress is involved in the pathogenesis of the PMD patients with PLP1 missense mutations, and a higher susceptibility to ER stress was observed in PMD1 iPSC-derived OLs than in those derived from PMD2, which is consistent with the more severe phenotypes of the PMD1 patient compared with the PMD2 patient.

### Increased Apoptosis Is Observed in PMD iPSC-Derived Oligodendrocytes

In addition to their susceptibility to ER stress, the PMD iPSC-derived OLs showed significant morphological differences, as revealed by O4 staining, such as scattered O4 staining in their processes compared with control iPSC-derived OLs, which exhibited uniform O4 staining in their processes (Figure 5A). Thus, to investigate the apoptotic processes of PMD iPSC-derived OL lineage cells, we examined the expression of cleaved caspase-3 (apoptotic marker) in O4<sup>+</sup>-immature OLs and MBP<sup>+</sup>-mature OLs via immunostaining. Some of the PMD iPSC-derived OLs that showed scattered O4 staining in their processes were positive for cleaved caspase-3 (Figure 5B). The numbers of cleaved caspase-3<sup>+</sup> cells in both PMD1 and PMD2 iPSC-derived immature OLs and mature OLs were significantly increased compared with those derived from control iPSCs (Figure 5C). We next performed immunocytochemistry for KI67 and OLIG2. We found that the proportion of OLIG2<sup>+</sup> cells and KI67<sup>+</sup> cells among OLIG2<sup>+</sup> cells were unchanged between PMD and control samples, suggesting that the compensatory proliferation of OPCs for increased apoptosis in PMD iPSC-derived OLs is unlikely (Figures S2A and S2B). Therefore, although

(E) Representative low-magnification images of the immunocytochemistry of three neural lineage cells (neurons:  $\beta$ III tubulin; astrocytes: GFAP; oligodendrocytes: O4). The scale bar represents 100  $\mu$ m.

(F) Quantitative analysis of the percentages of three neural lineage cells in control-iPSCs (201B7, WD39, and TIG121)-derived neurospheres ( $n = 9$ ; mean  $\pm$  SEM; independent experiments).

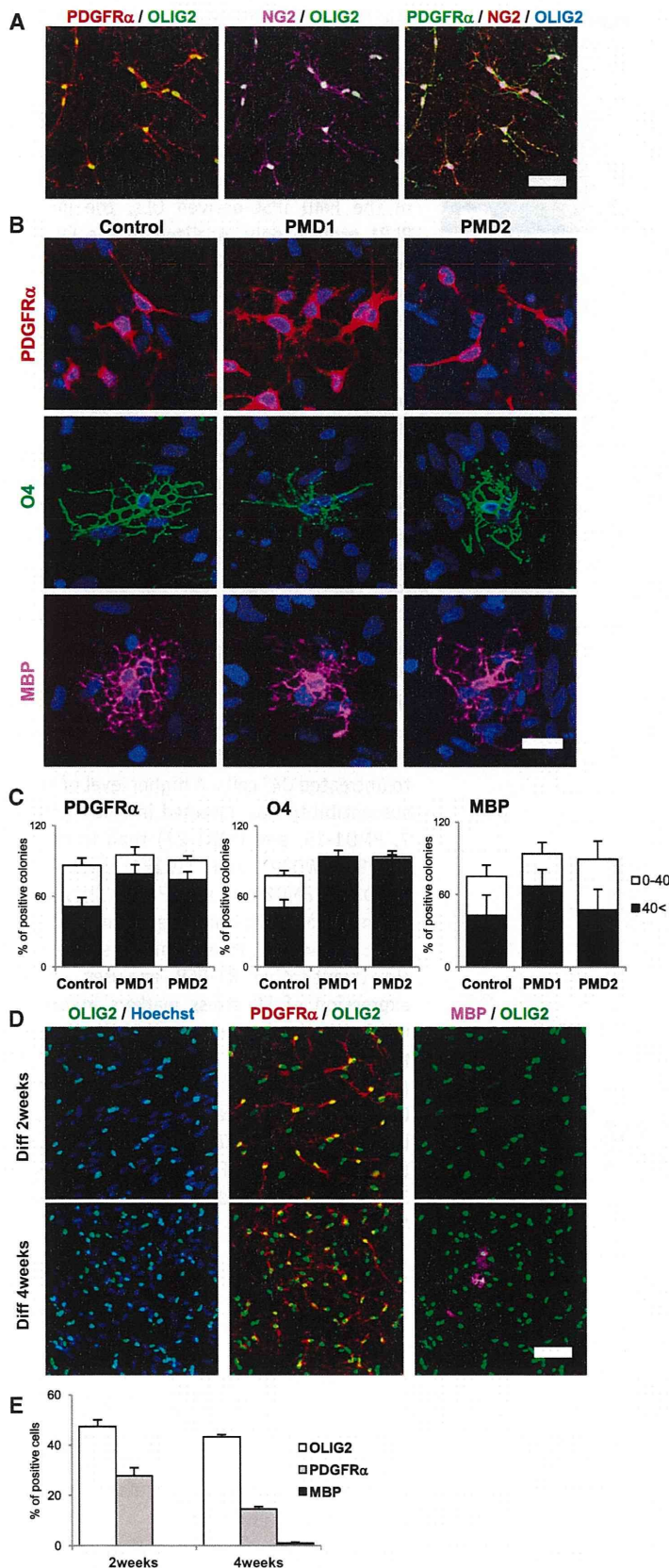


**Figure 3. Differentiation Potential of Human iPSCs into Oligodendrocytes**

(A) Representative image of immunocytochemistry for OPC markers (PDGFR $\alpha$  and NG2). OPCs were positive for both PDGFR $\alpha$  and NG2. The scale bar represents 50  $\mu$ m.

(B) Representative image of immunocytochemistry of differentiated neurospheres using markers for OL lineage cells. Both control and PMD iPSCs differentiated into PDGFR $\alpha$ <sup>+</sup>-OL progenitor cells (OPCs), O4<sup>+</sup>-immature OLs (immature OLs), and MBP<sup>+</sup>-mature OLs (mature OLs). The scale bar represents 20  $\mu$ m.

(C) Quantitative analysis of the differentiation efficiency into OL lineage cells. The numbers of neurosphere colonies containing more than 40 marker-positive cells ( $\geq 40$  cells; oligodendrocyte [++]), those containing less than 40 marker-positive cells (1–39 cells oligodendrocyte [+]), and those without marker-positive cells (oligodendrocyte [–]) were counted and are presented as the percentage of total neurosphere colonies. Oligodendrocyte (++) neurosphere colonies and oligodendrocyte (+) neurosphere colonies are indicated by black and white bars, respectively (PDGFR $\alpha$ , n = 6; O4, n = 6; MBP, n = 4; mean  $\pm$  SEM; independent experiments). No significant difference was detected among control (201B7, WD39, and TIG121) and PMD iPSCs (PMD1-7, PMD1-15, and PMD1-27 and PMD2-6, PMD2-10, and PMD2-22)-derived OL lineage cells (p > 0.05; Mann-Whitney's U test).

(D) Representative image of immunocytochemistry for OLIG2, PDGFR $\alpha$ , and MBP after 2 or 4 weeks differentiation of control-iPSC-derived second neurospheres containing more than 40 OLIG2-positive cells. The scale bar represents 50  $\mu$ m.

(E) Quantitative data of the percentages of PDGFR $\alpha$ <sup>+</sup> cells/OLIG2<sup>+</sup> cells and MBP<sup>+</sup> cells/OLIG2<sup>+</sup> cells (after 2 or 4 weeks of differentiation) in control-iPSC (201B7, WD39, and TIG121)-derived neurospheres containing more than 40 OLIG2-positive cells. (n = 3; mean  $\pm$  SEM; independent experiments). After 2 and 4 weeks of differentiation, OLIG2<sup>+</sup> and PDGFR $\alpha$ <sup>+</sup> OPCs were abundantly observed. After 4 weeks of differentiation, small numbers of MBP<sup>+</sup> mature OLs appeared.

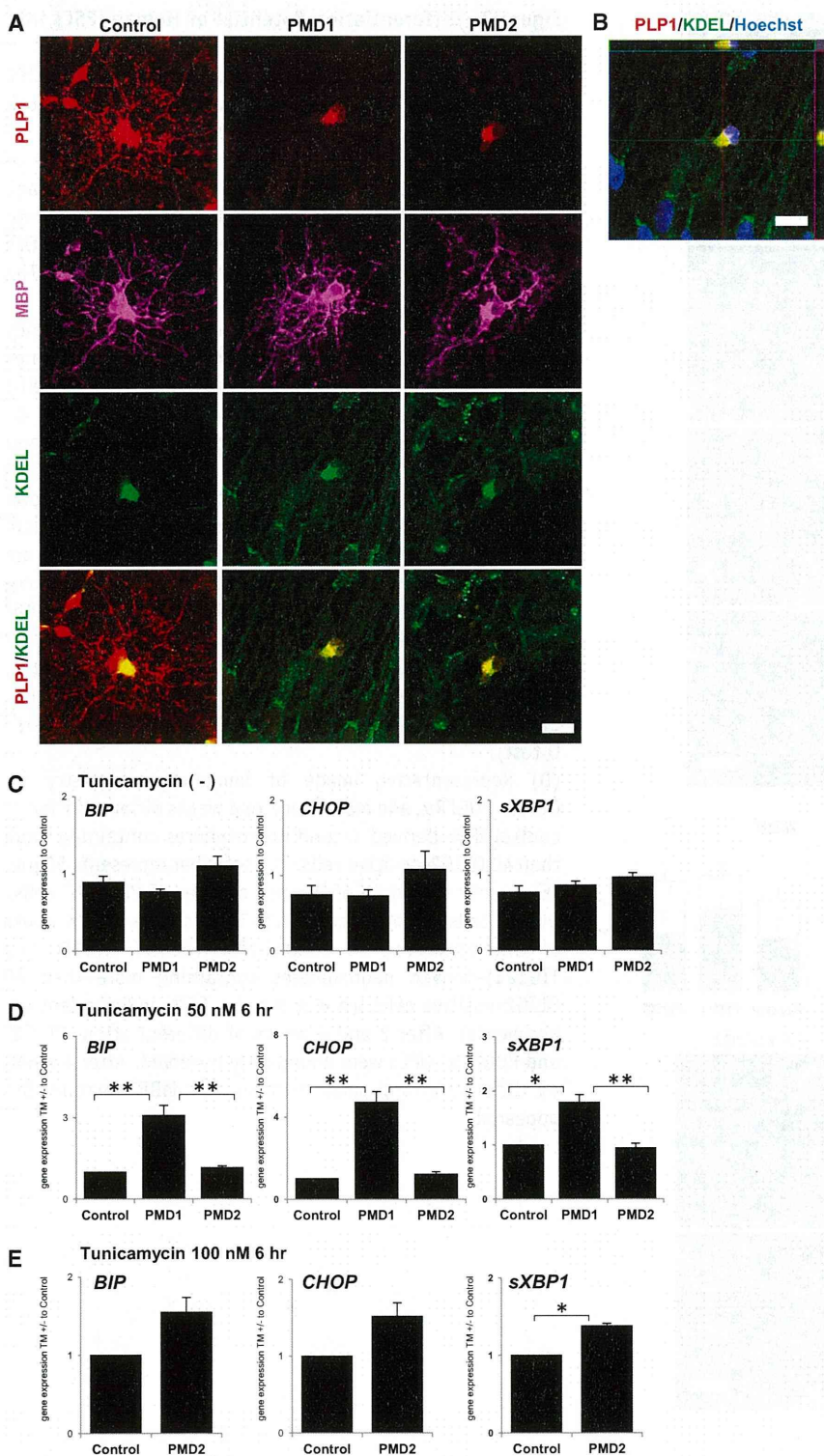


**Figure 4. Involvement of ER Stress in PMD-Derived Oligodendrocytes**

(A) Representative immunocytochemistry image for PLP1, the OL marker MBP, and the ER marker KDEL. In the control iPSC-derived mature OLs, the PLP1 protein localized to both the ER (KDEL) and membrane, whereas in the PMD iPSC-derived OLs, the mutant PLP1 protein only localized to the ER. The scale bar represents 20  $\mu$ m.

(B) Three-dimensional image of mature OLs derived from PMD1 iPSCs showing colocalization of the mutant PLP1 protein and KDEL via confocal laser scanning microscopy. The scale bars represent 20  $\mu$ m.

(C) Quantitative RT-PCR analyses of the expression of ER stress markers in O4<sup>+</sup> cells. The data are presented as the expression relative to that in iPSCs. No significant differences were observed between the control iPSC (201B7, WD39, and TIG121) and PMD iPSC (PMD1-7, PMD1-15, and PMD1-27 and PMD2-6, PMD2-10, and PMD2-22)-derived cells (n = 5; mean  $\pm$  SEM; independent experiments; t test).

(D) Quantitative RT-PCR analyses of the expression of ER stress markers in tunicamycin-treated (50 nM; 6 hr) O4<sup>+</sup> cells relative to untreated O4<sup>+</sup> cells. A higher level of stress susceptibility was detected in PMD1 (PMD1-7, PMD1-15, and PMD1-27) than in control (201B7, WD39, and TIG121) and PMD2 (PMD2-6, PMD2-10, and PMD2-22)-derived OLs (n = 5; mean  $\pm$  SEM; independent experiments; \*p < 0.05; \*\*p < 0.01; Mann-Whitney's U test).

(E) Quantitative RT-PCR analyses of the expression of ER stress markers in tunicamycin-treated (100 nM; 6 hr) O4<sup>+</sup> cells relative to untreated O4<sup>+</sup> cells. PMD2 iPSC (PMD2-6, PMD2-10, and PMD2-22)-derived OLs showed significantly higher expression levels of spliced XBP1 than control iPSC (201B7, WD39, and TIG121)-derived OLs (n = 3; mean  $\pm$  SEM; independent experiments; \*p < 0.05; t test).

the differentiation efficiency into oligodendrocyte lineage cells was unchanged between PMD and control (Figure 3C), considering that anti-O4 and anti-MBP antibodies stain both apoptotic and live OLs (Figures 5A and 5C), the

increased levels of apoptosis resulted in decreased numbers of live OLs in PMD iPSC-derived cultures.

Because previous reports have indicated the neurotrophic actions of PLP1 (Griffiths et al., 1998; Yin et al.,

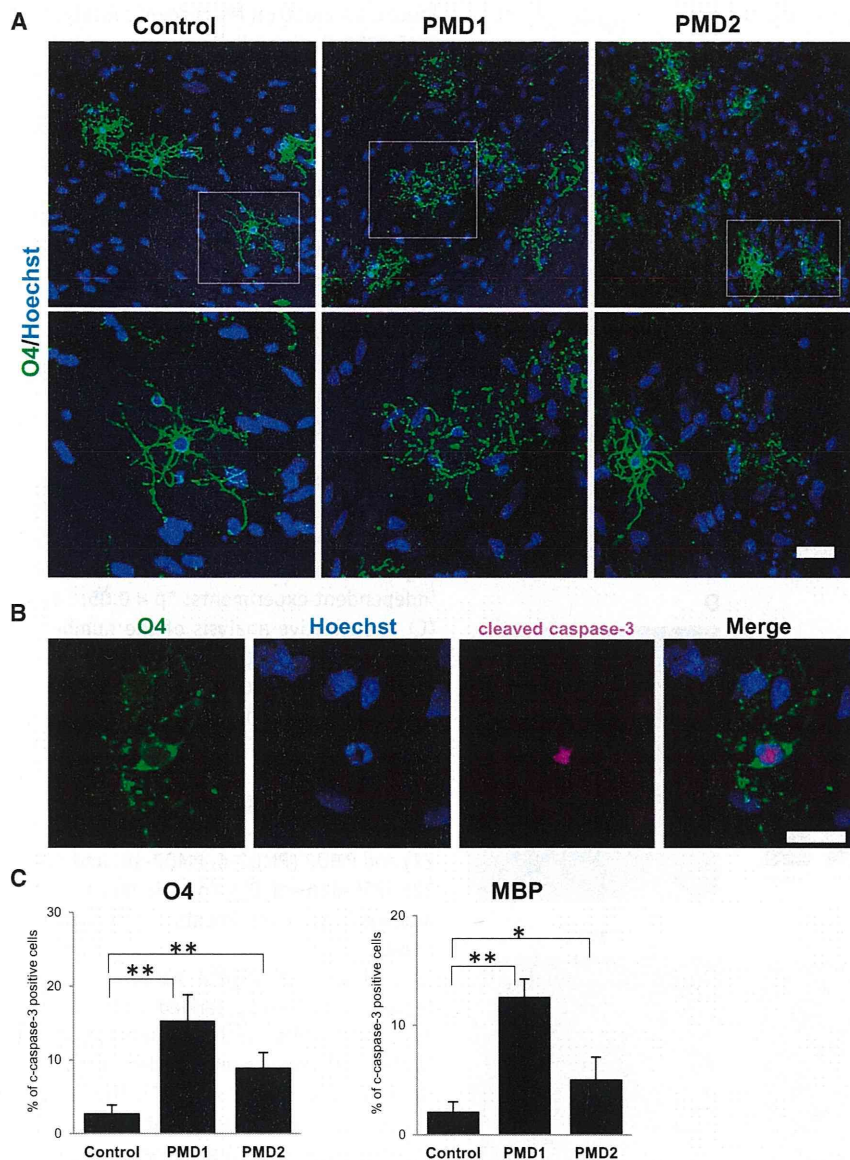


**Figure 5. Enhanced Apoptosis in PMD iPSC-Derived Oligodendrocytes**

(A) Morphological differences in OLs. Immunocytochemical analysis of iPSC-derived OLs for OLs marker (O4) and nuclei (Hoechst). The OLs showed a uniform appearance in the control iPSC-derived cells but showed scattered morphologies in the PMD iPSC-derived cells. The scale bar represents 40  $\mu$ m.

(B) Representative immunocytochemical images of apoptotic OLs using markers for apoptosis (cleaved caspase-3) and OLs (O4). OLs (O4<sup>+</sup> or MBP<sup>+</sup>) that were both positive for cleaved caspase-3 and showed nuclear condensation or fragmentation were considered apoptotic OLs. The scale bar represents 40  $\mu$ m. c-caspase-3, cleaved caspase-3.

(C) Quantitative analysis of the number of apoptotic OLs. The number of apoptotic cells was higher in the PMD1 (PMD1-7, PMD1-15, and PMD1-27) and PMD2 iPSC (PMD2-6, PMD2-10, and PMD2-22)-derived OLs than control iPSC (201B7, WD39, and TIG121)-derived OLs (n = 9; mean  $\pm$  SEM; independent experiments; \*p < 0.05; \*\*p < 0.01; Mann-Whitney's U test).

2006), we next investigated whether apoptosis was induced in PMD patient-derived neurons. However, no cleaved caspase-3<sup>+</sup> neurons derived from either control or PMD iPSCs were observed (Figure S2C), suggesting that this increased apoptosis was specific to oligodendrocyte lineage cells in PMD in our iPSC-derived cultures.

#### Abnormal Myelin Structures and ER Morphologies Were Detected by Electron Microscopic Analysis

Finally, we focused on the myelinating properties of PMD iPSC-derived OLs, which represent the most characteristic pathogenic feature of PMD. Because different types of neural cells, including neurons and astrocytes, in addition to OLs, were derived in our cultures, neuron-glia interactions

could be observed and neuron myelination by the iPSC-derived OLs could be analyzed *in situ*. In immunocytochemical analysis of MBP and NF200 (neurofilament marker), parts of the neurofilament<sup>+</sup> neurites were wrapped by the MBP<sup>+</sup> process of iPSC-derived oligodendrocytes (Figure S3A). Thus, to evaluate the histological abnormality of the myelin structures *in vitro*, we performed transmission electron microscopy (TEM) analysis of ultrathin sections of the differentiated cells. The results showed that myelin structures with or without axons could be observed via TEM. Considering the neuronal processes wrapped by the MBP<sup>+</sup> process of iPSC-derived OLs observed through immunocytochemistry, some of the axonal structures could have been lost during the fixation process for TEM.

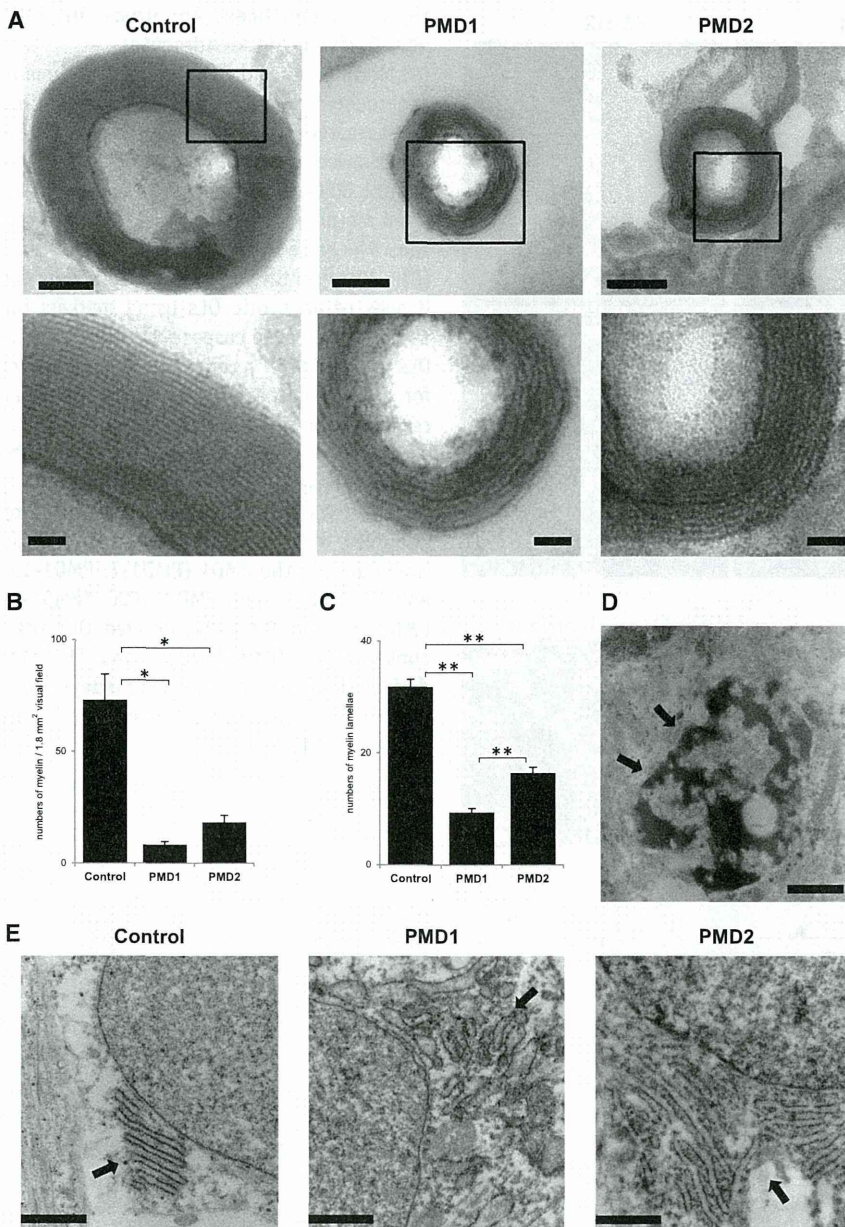


**Figure 6. Electron Microscopic Analysis of PMD iPSC-Derived Cells**

(A) TEM of iPSC-derived cells. The maximum number of normal myelin lamella was greater than 30 in the control iPSC-derived myelin sheaths. In contrast, a limited number of myelin lamella was observed in the PMD iPSC-derived myelin sheaths. High-magnification images are also shown in the lower panel. The scale bars represent 100 nm (upper panels) and 20 nm (lower panels).

(B) Quantitative analysis of the numbers of myelin structures. We counted the numbers of myelin structures per visual field of EM images (approximately 1.8 mm<sup>2</sup>) for the myelination frequency. The frequency of myelin formation was significantly decreased in both PMD1 (PMD1-7, PMD1-15, and PMD1-27) and PMD2 (PMD2-6, PMD2-10, and PMD2-22) iPSC-derived OLs (n = 3; mean ± SEM; independent experiments; \*p < 0.05; t test).

(C) Quantitative analysis of the numbers of myelin lamellae. We counted the numbers of major dense lines per myelinated fiber for the thickness of myelin, and the average of the numbers of myelin lamellae in the top ten myelin sheaths are presented. The thickness of the myelin sheath was greatly reduced in both PMD1 (PMD1-7, PMD1-15, and PMD1-27) and PMD2 (PMD2-6, PMD2-10, and PMD2-22) iPSC-derived OLs (n = 3; mean ± SEM; independent experiments; \*\*p < 0.01; t test).

(D and E) Histological abnormalities detected in PMD iPSC-derived cells via TEM. Apoptotic cells with fragmented nuclei (arrow in D) were frequently detected among the PMD-iPSC-derived cells (D). The scale bar represents 1 μm. Dilations of ER intermembrane spaces were also observed (E). The scale bars represent 0.5 μm.

Although we stained with antibodies against NAV1.6 (nodes) and CASPER (paranodes), we could not detect any significant staining in our cultures. This may suggest immature myelination in the present culture conditions.

Notably, mature myelin structures with thick myelin lamella ~30 layers were observed in the control cultures. In contrast, in the PMD iPSC-derived cultures, a limited number of myelin structures with thin myelin lamella ~15 layers were observed (Figure 6A). The frequency of myelin formation and thickness of the myelin sheath were significantly decreased in both PMD1 and PMD2 iPSC-derived OLs (Figures 6B and 6C).

In addition, several types of histological abnormalities were detected in the PMD cells. Apoptotic cells exhibiting nuclear condensation were frequently observed among the PMD iPSC-derived cells, in contrast to that observed in those derived from control iPSCs (Figure 6D). Moreover, aberrant ER morphologies, such as dilation of the ER intermembrane space (Fan et al., 2013; Lim et al., 2011), were found in the PMD iPSC-derived cells (Figure 6E). These results indicate that PMD iPSC-derived OLs develop a poor myelin structure and subsequently die, supporting the involvement of ER stress in the pathogenesis of PMD.



## DISCUSSION

In this study, we established PMD-specific human iPSCs from two patients with different clinical severity and different missense mutations of *PLP1*. One mutation is in the transmembrane domain (PMD1) and the other is in the extracellular domain (PMD2), both of which differ from those in the previously reported PMD animal models. And we generated patient-specific OLs. This model enables an investigation of the correlations between the molecular pathophysiology of PMD and various cell biological phenomena, including OL differentiation, myelination, and apoptosis in patient-derived live OLs through morphological, biochemical, and molecular biological methods. These analyses could not be achieved using conventional disease models.

Although there are several reported methods for inducing OPCs from human ESCs (Hu et al., 2009; Izrael et al., 2007; Kang et al., 2007), these methods have difficulties in reproducibility, making it difficult to obtain sufficient amounts of mature OLs for analysis. In the present study, we developed an improved neural differentiation protocol for human pluripotent stem cells by utilizing an EB-neurosphere method involving dual Smad inhibition in combination with a GSK3 inhibitor to facilitate differentiation into NS/PCs more efficiently and reproducibly. In addition, the use of T3, ciliary neurotrophic factor (CNTF), and leukemia inhibitory factor (LIF) was beneficial for differentiation into OLs. Using this method, we achieved stable differentiation of several human iPSC clones into OLs in a similar manner to that reported in a recent study (Wang et al., 2013). Remarkably, our culture procedure enabled recapitulation of myelin formation in human iPSC (hiPSC)-derived neurites and OLs in vitro in a single-culture system without coculturing with other cells, such as rodent hippocampal neurons, as previously reported (Kang et al., 2007). Thus, this study reports a successful in vitro myelination assay using human iPSC-derived neurons and OLs.

Another important finding of this study was that the differentiation of PMD iPSCs into OLs well-recapitulated the progression of PMD pathogenesis in vitro. Although the PMD-specific iPSCs induced abundant MBP<sup>+</sup> mature OLs, myelination was substantially less frequent and limited lamella formation was observed. These results suggest that incomplete maturation and limited survival of OLs rather than a failure to differentiate into OLs is responsible for PMD pathogenesis. However, the cause of OL degeneration and dysmyelination observed in PMD is unclear. Some previous reports have demonstrated the involvement of ER stress in the pathogenesis of PMD associated with missense mutations in the *PLP1* gene. Analyses using cell lines, such as cos7 cells transfected with wild-type or

mutant *PLP1* genes, have shown that wild-type PLP1 protein is synthesized in the ER and transported to the cell surface, whereas mutant PLP1 proteins are arrested in the secretory pathway at an early stage and accumulate in the ER (Gow et al., 1994). In the CNS of PMD model mice, such as *msd* and *rsh* mice, mutant PLP1 proteins are largely confined to the perinuclear region of OLs and involved in the UPR (Gow et al., 1998). These reports suggest the involvement of ER stress in PMD pathogenesis. In the present study, accumulation of misfolded mutant PLP1 proteins in the ER and high susceptibility to ER stresses in the PMD1 and PMD2 cells were observed. This increased susceptibility to ER stresses or other cellular response could have resulted in the apoptosis of PMD iPSC-derived OLs and immature/incomplete myelination.

In addition, we detected differences between PMD1 and PMD2 cells. The differences of susceptibility to ER stresses and the thickness of the myelin sheath were consistent with the different levels of clinical severity of the two patients. The correlations between different clinical severity, different missense mutations, and different pathogenic changes have not previously been reported by conventional disease models. These results suggest that this PMD model accurately recapitulates disease pathophysiology not only qualitatively but also in terms of the degree of disease progression, although how the different point mutations affect the degree of the observed phenotype must be clarified. Accordingly, we propose models for a “proof-of-concept” of PMD pathogenesis based on the endogenous mutations found in PMD iPSC-derived OLs. The present findings cannot be generalized to PMD as a whole because the more common *PLP1* duplication was not included; therefore, we will investigate the pathogenesis of PMD with *PLP1* duplications in the future.

The current study represents the a demonstration of pathogenic changes in PMD patients with *PLP1* missense mutations using disease-specific, human iPSC-derived OLs. This model faithfully reproduces the pathophysiology observed in the CNS of PMD patients, which is difficult to identify through conventional experiments. Moreover, our results demonstrate the usefulness of iPSC-derived OLs for the analysis of the pathogenic processes of dysmyelinating human neurological disorders and the development of novel therapeutic agents for their treatment.

## EXPERIMENTAL PROCEDURES

### Isolation of Human Skin Fibroblasts and Generation of iPSCs

HDFs from the dermis of a 1-year-old Japanese male patient and HDFs from the dermis of a 20-year-old Caucasian male patient (Coriell Institute: GM09546) were used to establish PMD1-iPSCs (PMD1-7, 1-15, and 1-27) and PMD2-iPSCs (PMD2-6, 2-10, and





2-22), respectively. Additional control cell lines used in this study included 201B7 (control A, established from HDFs [Cell Applications] from the dermis of a 36-year-old Caucasian female; Takahashi et al., 2007), WD39 (control B, established from HDFs from the dermis of a 16-year-old Japanese female; Imaizumi et al., 2012), and TIG121 (control C, established from HDFs from the dermis of an 8-month-old Japanese male [Japan Health Sciences Foundation]). All of the human iPSC clones were established through the retroviral transduction of four transcription factors (*SOX2*, *OCT4*, *KLF4*, and *c-MYC*) into HDFs as described previously (Takahashi et al., 2007) and evaluated based on the expression of pluripotent markers, the silencing of retroviral transgenes, and teratoma formation assays as described previously (Ohta et al., 2011). We used three clones for each group for further analysis: control (201B7, WD39, and TIG121), PMD1 (1-7, 1-15, and 1-27), and PMD2 (2-6, 2-10, and 2-22). The data from the three clones were combined in each figure, and the data are shown as the average of the three clones. All of the experimental procedures for iPSC production were approved by the ethics committee of the Keio University School of Medicine (approval number: 20-16-18).

### Culture and In Vitro Differentiation of Human iPSCs

hiPSCs were grown on mitomycin-C-treated SNL murine fibroblast feeder cells in gelatin-coated (0.1%) tissue culture dishes. The hiPSCs were maintained in standard hESC medium (Dulbecco's modified Eagle's medium [DMEM]/F12 [Sigma] containing 20% KnockOut serum replacement [KSR; Life Technologies], nonessential amino acids [NEAA], 0.1 mM 2-mercaptoethanol [Sigma], and 4 ng/ml fibroblast growth factor 2 [FGF-2] [PeproTech]) at 37°C in a humidified atmosphere of 3% CO<sub>2</sub>.

For in vitro differentiation, iPSC colonies were detached from the feeder layers in bloc using a dissociation solution (0.25% trypsin, 100 µg/ml collagenase IV [Invitrogen], 1 mM CaCl<sub>2</sub>, and 20% KSR; day 0) and cultured in suspension in bacteriological dishes to form EBs in a humidified atmosphere of 3% CO<sub>2</sub>. From day 1 to 4 of EB formation, 3 µM dorsomorphin (Sigma), 3 µM SB431542 (Tocris Bioscience), and 3 µM BIO ((2'Z, 3'E)-6-bromoindirubin-3'-oxime; Sigma) were added. In addition, 1 µM retinoic acid (Sigma) and 1 µM purmorphamine (Calbiochem) were added on days 4 and 7, respectively, and maintained thereafter until day 16 (EB dissociation). The medium was changed every 2 days. On day 16, the EBs were enzymatically dissociated into single cells using TrypLE Select (Life Technologies), and the dissociated cells were cultured in suspension at a density of 1 × 10<sup>5</sup> cells/ml in proliferation medium consisting of serum-free medium (media hormone mix [MHM]; Okada et al., 2008) supplemented with 2% B27 supplement (Invitrogen), NEAA, 1 µM purmorphamine, 60 ng/ml T3 (Sigma), 10 ng/ml PDGF-AA (PeproTech), 20 ng/ml FGF, 10 ng/ml epidermal growth factor (PeproTech), 10 ng/ml insulin growth factor 1, and 10 ng/ml neurotrophin-3 (R&D Systems) in a humidified atmosphere of 5% CO<sub>2</sub>. The medium was changed every 4~6 days for approximately 15~20 days to form the first neurospheres. To passage neurospheres, the first neurospheres were dissociated in the same manner as described above and cultured at a density of 1 × 10<sup>5</sup> cells/ml in proliferation medium without purmorphamine for approximately 15~20 days. To assay neurosphere differentia-

tion, undissociated 5~7 neurospheres were plated onto coverslips 10 mm in diameter coated with poly-L-ornithine (Sigma) and growth-factor-reduced Matrigel (50× dilution, thin coated; Invitrogen), and cultured in differentiation medium that consisted of MHM supplemented with 2% B27 supplement, NEAA, 60 ng/ml T3, 10 ng/ml hLIF (Millipore), and 25 ng/ml CNTF (R&D Systems) for 2~6 weeks in a humidified atmosphere of 5% CO<sub>2</sub>. Half of the medium was changed every 2 or 3 days. For the quantitative analysis of the differentiation efficiency into OL lineage cells, the numbers of neurosphere colonies containing more than 40 marker-positive cells (≥ 40 cells, oligodendrocyte [+]), those containing less than 40 marker-positive cells (1~39 cells, oligodendrocyte [+]), and those without marker-positive cells (oligodendrocyte [-]) were counted and are presented as the percentage of total neurosphere colonies. To examine the expression of ER-stress markers, O4<sup>+</sup> differentiated cells were purified 4 weeks after the attachment of the neurospheres using MACS technology with an anti-O4 antibody.

### Direct Sequencing and Pyrosequencing Analysis of the *PLP1* Gene

Genomic DNA was extracted from peripheral blood samples (leukocytes) from PMD1 and from HDFs and iPSCs from both PMD1 and PMD2. For direct sequencing of the mutations in the *PLP1* gene in PMD1, fragments of the promoter regions (5' UTR) and all seven exons of the *PLP1* gene were amplified via PCR. The PCR primers and cycling conditions employed for direct sequencing are listed in Table S1. For pyrosequencing analysis of the mutations in the *PLP1* gene in HDFs and iPSCs, fragments containing the PMD1 mutation (c.757 T > A in exon 6) and PMD2 mutation (c.643 C > T in exon 5) were amplified via PCR using forward primers and biotinylated reverse primers. Pyrosequencing analyses were performed following the manufacturer's instructions (PyroMark Q24; QIAGEN). The PCR primers and cycling conditions applied for pyrosequencing analysis are listed in Table S2.

### RNA Isolation and RT-PCR

RNA isolation and real-time quantitative RT-PCR were performed as previously described using SYBR Premix ExTaq II and the MX3000P Real-Time PCR system (Stratagene; Okada et al., 2004, 2008). The amount of cDNA was normalized to that of human-specific  $\beta$ -ACTIN mRNA.

For the analysis of the expression of retroviral transgene in iPSCs, HDFs 7 days after the retroviral introduction (day 11 of the protocol) of four genes (*SOX2*, *OCT4*, *KLF4*, and *c-MYC*) were used as the positive control (*SOX2* tg, *OCT4* tg, *KLF4* tg, and *c-MYC* tg). The data are presented as the copy numbers of mRNA for each transgene. As for the analyses of *NANOG*, *SOX1*, *BRACHYURY*, *SOX17*,  $\beta$ III tubulin, *GFAP*, *CNP*, and ER stress marker (*BIP*, *CHOP*, and *spliced XBP1*), data are presented as the relative expression to that in control. The applied primer sequences and PCR cycling conditions are listed in Table S3.

### Immunocytochemical Analysis

For immunocytochemical analysis, cells were fixed with 4% paraformaldehyde for 30 min at room temperature. After blocking in



blocking buffer (PBS containing 10% normal goat or donkey serum and 0.3% Triton X-100) for 1 hr at room temperature, the cells were incubated with primary antibodies at 4°C overnight. For O4 staining, we used blocking buffer without Triton X-100. After three washes with PBS, the cells were incubated with Alexa 488-, Alexa 555-, or Alexa 647-conjugated secondary antibodies (Life Technologies) for 1 hr at RT. Nuclei were stained with 10 µg/ml Hoechst 33258 (Sigma). After washing with PBS, the cells were mounted on slides and examined with a universal fluorescence microscope (Axiophoto; Carl Zeiss) or confocal laser scanning microscope (LSM700; Carl Zeiss). The primary antibodies used in these analyses were as follows: NANOG (1:100; ReproCELL), OCT4 (1:500; Santa Cruz Biotechnology), OLIG2 (1:1,000; R&D Systems), PDGFR $\alpha$  (1:2,000; Santa Cruz Biotechnology), NG2 (1:2,000; Millipore), O4 (1:5,000; Millipore), MBP (1:1,000; Serotec),  $\beta$ -III-tubulin (1:1,000; Sigma), NF200 (1:1,000, Millipore), GFAP (1:4,000, Dako), KDEL (Abcam), PLP1 (1:30,000; gifted from Masayuki Itoh [National Center of Neurology and Psychiatry] recognizes PLP1, but not DM20), KI67 (1:10,000, Abcam), and cleaved caspase 3 (1:1,000, Cell Signaling Technology).

### Teratoma Assay

Undifferentiated iPSCs ( $5 \times 10^5$  cells) were injected into the testes of 8-week-old male nonobese diabetic (NOD)/severe combined immunodeficiency (SCID) mice (Charles River Laboratories) as described previously (Ohta et al., 2011). Eight weeks after injection, the resultant tumors were dissected and fixed with 4% paraformaldehyde. Paraffin-embedded tissue sections were produced, and hematoxylin and eosin (H&E) staining was performed. Images were obtained using a BZ-9000 microscope (Keyence).

### Transmission Electron Microscopy

For TEM analysis, neurospheres and cells in dishes were fixed with 2.5% glutaraldehyde in 50 mM phosphate buffer (PB) overnight at 4°C. After washing twice in 0.1 M PB, these samples fixed with 1% osmium tetroxide for 90 min, dehydrated through ethanol, and embedded in Epon. The neurospheres were dissected and fixed on the stage, followed by the preparation of ultrathin sections with a thickness of 70 nm using an ultramicrotome (Leica Microsystems). The sections were subsequently stained with uranyl acetate and lead citrate for 10 and 12 min, respectively. Finally, the sections were observed under a transmission electron microscope (JEOL model 1230), and images were captured with Digital Micrograph 3.3 (Gatan). For the quantitative analysis of myelination, the number of myelin lamellae, which is the number of major dense lines per myelinated fibers, was counted to assess myelin thickness and the number of myelinated fibers per visual field of electron microscopy (EM) images (approximately 1.8 mm<sup>2</sup>) was counted to assess myelination frequency.

### SUPPLEMENTAL INFORMATION

Supplemental Information includes three figures and three tables and can be found with this article online at <http://dx.doi.org/10.1016/j.stemcr.2014.03.007>.

### ACKNOWLEDGMENTS

We are grateful to Prof. F. Urano (Washington University School of Medicine) for valuable comments and analysis of ER stress, Prof. M. Amagai (Keio University) for skin biopsies, I. Kuki (Osaka City General Hospital) for providing patient medical information, M. Itoh (National Center of Neurology and Psychiatry) for providing PLP1 antibody, T. Nagai (Keio University) for assistance with the TEM analyses, N. Kuzumaki (Keio University) for technical assistance, and all of the members of H.O.'s laboratory for their encouragement and support. This work was supported by funding from the Project for the Realization of Regenerative Medicine and Support for Core Institutes for iPSC Cell Research from the Ministry of Education, Culture; Support for the Core Institutes for iPSC Cell Research from the Ministry of Education, Culture, Sports, Science and Technology of Japan (MEXT; to H.O.); and a Grant-in-Aid for the Global COE Program from MEXT to Keio University. This work was also supported by a Grant-in-Aid for Young Scientists (B) from MEXT, a Keio University Grant-in-Aid for the Encouragement of Young Medical Scientists to Y.K.-N. from the Kanrinmaru-Project at Keio University, a Grant-in-Aid for Young Scientists (A) and a Grant-in-Aid for Scientific Research on Innovative Areas (Foundation of Synapse Neurocircuit Pathology) from MEXT, and JST-CIRM Collaborative Research Program funding awarded to Y.O. H.O. is a scientific consultant for SanBio, Inc., Eisai, Co., Ltd., and Daiichi Sankyo, Co., Ltd. M.S. and A.N. are employed by Takeda Pharmaceutical Company Limited. S.Y. is a member without salary of the scientific advisory boards of iPierian, iPSC Academia Japan, Megakaryon Corporation, and HEALIOS K. K. Japan.

Received: October 8, 2013

Revised: March 20, 2014

Accepted: March 20, 2014

Published: April 24, 2014

### REFERENCES

- Fan, J., Long, H., Li, Y., Liu, Y., Zhou, W., Li, Q., Yin, G., Zhang, N., and Cai, W. (2013). Edaravone protects against glutamate-induced PERK/EIF2 $\alpha$ /ATF4 integrated stress response and activation of caspase-12. *Brain Res.* 1519, 1–8.
- Gencic, S., Abuelo, D., Ambler, M., and Hudson, L.D. (1989). Pelizaeus-Merzbacher disease: an X-linked neurologic disorder of myelin metabolism with a novel mutation in the gene encoding proteolipid protein. *Am. J. Hum. Genet.* 45, 435–442.
- Gow, A., and Lazzarini, R.A. (1996). A cellular mechanism governing the severity of Pelizaeus-Merzbacher disease. *Nat. Genet.* 13, 422–428.
- Gow, A., Friedrich, V.L., Jr., and Lazzarini, R.A. (1994). Many naturally occurring mutations of myelin proteolipid protein impair its intracellular transport. *J. Neurosci. Res.* 37, 574–583.
- Gow, A., Gragerov, A., Gard, A., Colman, D.R., and Lazzarini, R.A. (1997). Conservation of topology, but not conformation, of the proteolipid proteins of the myelin sheath. *J. Neurosci.* 17, 181–189.
- Gow, A., Southwood, C.M., and Lazzarini, R.A. (1998). Disrupted proteolipid protein trafficking results in oligodendrocyte apoptosis